Liquid Crystals
Publication details, including instructions for authors and subscription information:
http://www.informaworld.com/smpp/title~content=t713926090

Synthesis and thermotropic behaviour of imidazole-terminated liquid crystals

Supacharee Roddecha[a]; Mitchell Anthamatten[a]
[a] Department of Chemical Engineering, University of Rochester, Rochester, NY, USA

Online publication date: 23 April 2010

To cite this Article Roddecha, Supacharee and Anthamatten, Mitchell(2010) 'Synthesis and thermotropic behaviour of imidazole-terminated liquid crystals', Liquid Crystals, 37: 4, 389 — 397
To link to this Article: DOI: 10.1080/02678291003632611
URL: http://dx.doi.org/10.1080/02678291003632611

Liquid Crystals,
Vol. 37, No. 4, April 2010, 389–397

Taylor & Francis
Taylor & Francis Group

Synthesis and thermotropic behaviour of imidazole-terminated liquid crystals

Supacharee Roddecha and Mitchell Anthamatten*

Department of Chemical Engineering, University of Rochester, Rochester, NY 14627, USA

(Received 12 November 2009; final version received 18 January 2010)

Two novel liquid crystals containing terminal imidazole groups (**Imi-COOH** and **Imi-DAH**) were designed and synthesised. **Imi-COOH** exhibits a high-temperature monotropic smectic mesophase that is substantially stabilised by hydrogen bonding between acid and imidazole end-groups. Despite its rigid diacylhydrazine core, which offers the capability of forming lateral hydrogen bonds, **Imi-DAH** exhibits a nematic mesophase. Fourier transform infrared analysis suggested that the terminal imidazole group interferes with lateral hydrogen bonding between diacylhydrazine cores and destabilises the smectic mesophase. Future studies will examine how proton transport is affected by anisotropic mesophases.

Keywords: thermotropic liquid crystals; imidazole; hydrogen bonding; smectic; proton exchange membranes; diacylhydrazines

1. Introduction

The self-organisation of functional liquid crystals (LCs) into anisotropic nematic, smectic and columnar mesophases is driven by molecular shape and intermolecular interactions. Recent research has been aimed at developing soft, organic mesophases with enhanced two-dimensional and one-dimensional ion conductivity [1–8]. These studies recognise that soft materials with high ion conductivity will play pivotal roles in emerging applications such as electrochromic displays, sensors, electroactive artificial muscles and energy storage devices. However, ion-transport through anisotropic LC phases is complex and poorly understood. Ion transport depends on many factors including the type of mesophase, the concentration of ion-conducting groups and the molecular mobility of the ion-conductive sites.

Strategies to engineer materials with enhanced ion conductivity have involved both liquid crystallinity and microphase segregation. As an example, smectic ordering of LCs containing ion-conductive (ethylene oxide) tails results in mesophases with alternating ion-conductive and insulating layers [4, 6]. The mesogens effectively concentrate ion-conductive tails between the insulating cores, thereby enhancing in-plane ion transport. Similar anisotropic properties have been reported within liquid-crystalline polymer phases [2, 6]. In these cases, monomers were synthesised to contain both ion-conductive and polymerisable tail groups. Monomer LCs were then shear-aligned into macroscopically aligned mesophases and were subsequently UV-polymerised. Anisotropy can also be introduced using block copolymers to direct the assembly of functional groups into channels [3, 9]. For example, block repulsion in poly (styrene)-block-poly(vinyl pyridine) copolymers directs ethylene oxide oligomers into aligned channels. Here, the glassy nature of the poly(styrene) phase offers mechanical support, and the high segmental motion of oligomers promotes ion transport.

Despite these modest successes, there are few efforts to use LC ordering to promote proton conductivity. Protogenic LCs may offer an approach to new anhydrous fuel cell membranes. Proton exchange membranes (PEMs) that operate between 100 and 200°C, under low-humidity conditions, could have a major impact on fuel cell technologies. The current, state-of-the art, polymer electrolyte membrane consists of perfluorosulphonic acid materials such as Nafion®. Although these materials offer high proton conductivity (up to 0.5 s cm^{-1}), they can only be operated under hydrated conditions and, therefore, are limited to low temperatures (about 80°C). Recently, heterocyclic compounds such as imidazole have been investigated as a replacement for acidified PEMs. Small amounts of imidazole (about 10%) added to liquid sulphanilic acid improve conductivities by almost a factor of ten [10]. Since then, attempts to immobilise imidazole have focused on covalent attachment of imidazole heterocycles on to oligomer and polymer backbones [11–15]. Resulting materials exhibit proton conductivities up to about 10^{-3} s cm^{-1} in the anhydrous state. By comparing different polymers and architectures, these studies show that a low glass transition temperature and long flexible spacers are essential to achieve anhydrous proton transport. More importantly, such studies emphasise that achieving high proton conductivity in a polymeric system is a feasible goal.

*Corresponding author. Email: anthamatten@che.rochester.edu

ISSN 0267-8292 print/ISSN 1366-5855 online

DOI: 10.1080/02678291003632611
http://www.informaworld.com

This study takes an important step in evaluating liquid crystallinity as a strategy to develop anhydrous proton-conducting materials. The design and synthesis of two new imidazole-terminated mesogens containing diacylhydrazine cores is reported. Here, we discuss issues related to synthesis, chemical characterisation and phase behaviour of these protogenic LCs. The report will focus on how hydrogen bonding of the imidazole tail affects the LC phase stability.

2. Results and discussion

2.1 Mesogen design and synthesis

The molecular structures of targeted imidazole-terminated mesogens **Imi-DAH** and **Imi-COOH** are shown in Scheme 1. Both were designed to exhibit high-temperature smectic mesophases. **Imi-DAH** contains a rigid diacylhydrazine core, a long-chain hydrocarbon spacer and a terminal imidazole group. Lateral hydrogen bonding between diacylhydrazine cores is expected to support parallel alignment and stabilise smectic mesophases [16–19]. The core is connected to a long, tetradecane spacer to further promote high-temperature ordered phases and also to decouple the motion of the imidazole end-group from the ordered cores. Finally, the terminal 2-N-imidazole functional group is included as an anhydrous proton-conducting group. This functional group has been well studied and in the presence of an acid, imidazole acts as a Lewis base to support proton-hopping via a Grotthuss-like mechanism [20]. Free rotation of the imidazole ring around the C–S bond and the symmetry of the 2-substituted imidazole ring are further molecular design features that were included to maximise imidazole ring mobility while confined within a highly ordered mesophase.

Imi-COOH is similar to **Imi-DAH.** Both use long alkyl spacers to promote high-temperature mesophases, and both contain a freely rotating, terminal imidazole group. However **Imi-COOH** does not include a diacylhydrazine core. Instead, **Imi-COOH** bears a terminal benzoic acid group that is free to undergo end-to-end dimerisation between carboxylic acid groups (head-to-head), or hydrogen bonding between carboxylic acid groups and terminal imidazole groups (head-to-tail). Both bonding scenarios promote a layered structure and should support smectic mesophases.

Imi-DAH and **Imi-COOH** were obtained following the synthesis outlined in Scheme 1. Synthesis began with the reduction of tetradecanedioic acid into the corresponding diol **1**. One hydroxyl end-group is brominated to form **2**, and this product is coupled with *p*-hydroxy ethyl benzoate in the presence of a base to form **3**. The remaining hydroxyl group on **3** was converted to the corresponding bromide **4** using a one-pot, mild bromination approach [21]. Other attempts to selectively transform the hydroxyl group on **3** into a good leaving group failed, and these methods involved selective tosylation and strong bromination. These attempts resulted in unexpected side-products, difficult separation and unselective bromination. Following the mild bromination procedure, an imidazole group was attached by reaction of **4** with mercaptoimidazole. Finally, the ethylbenzoate end was hydrolysed to achieve imidazole-terminated carboxylic compound, 4-(14-mercaptyl imidazole tetradecyloxy) benzoic acid (**Imi-COOH**). The imidazole-terminated mesogen containing a diacylhydrazine core, 4-(14-mercaptyl imidazole tetradecyloxy) benzoic acid N'-(4-benzyloxyphenyl-2-carbonyl) hydrazide (**Imi-DAH)** was synthesised from a condensation reaction between **Imi-COOH** and hydrazide **7** through an acid chloride intermediate. Hydrazide **7** was obtained by reaction of hydrazine hydrate with ethyl-4-hydroxybenzoate **6**, which was prepared using a Williamson ether synthesis step.

2.2 LC phase behaviour

LC textures were observed using polarising optical microscopy (POM) and phase transition temperatures with associated enthalpy changes were investigated using differential scanning calorimetry (DSC). Variable temperature X-ray diffraction (XRD) was conducted to further examine high-temperature ordered phases.

Figures 1 and 2 display POM textures of **Imi-DAH** and **Imi-COOH** observed under crossed-polarisers during their second heating. While LC mesophases could not be clearly assigned based on these images alone, the data confirms that both mesogens exhibit high-temperature LC phases. Room temperature images of both compounds are consistent with a polydomain crystalline phase. Several cracks were observed at room temperature that likely resulted from stress accumulation during the prior cooling scan as crystallisation occurred. Upon heating, the compounds' transition to a liquid-crystalline phase occurred at about 130 and 170°C for **Imi-DAH** and **Imi-COOH,** respectively. A liquid-crystalline phase is evident from the high level of birefringence and observed fluid-flow characteristics. Upon further heating beyond 150°C, **Imi-DAH** transitioned to an isotropic phase. **Imi-COOH**, on the other hand, remained birefringent at temperatures even as high as 230°C. However, the POM texture of **Imi-COOH** distinctly changed between 190 and 230°C (see Figure 1), suggesting a transformation from one LC phase to another.

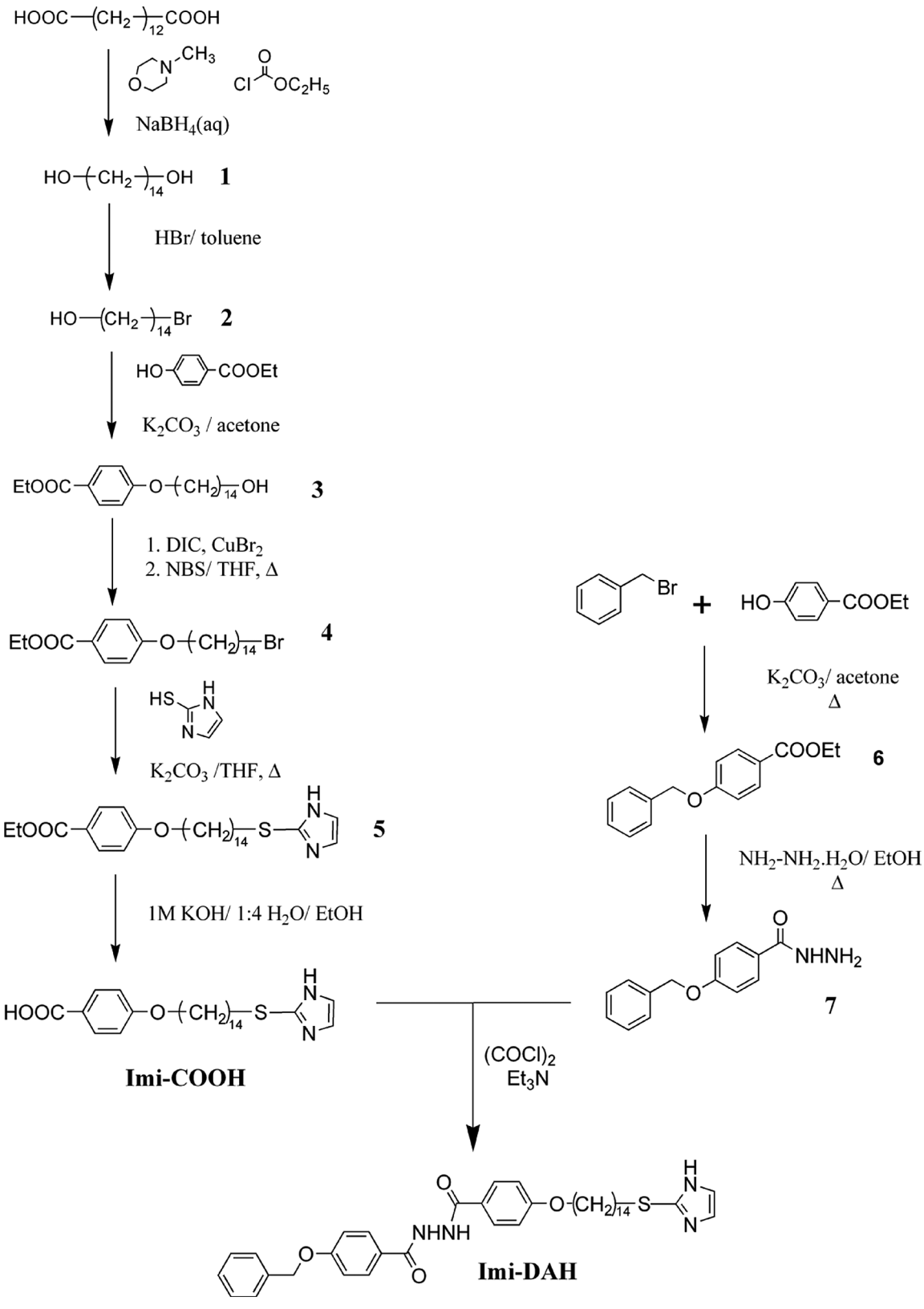

Scheme 1. Synthesis of liquid crystal mesogens **Imi-COOH** and **Imi-DAH**.

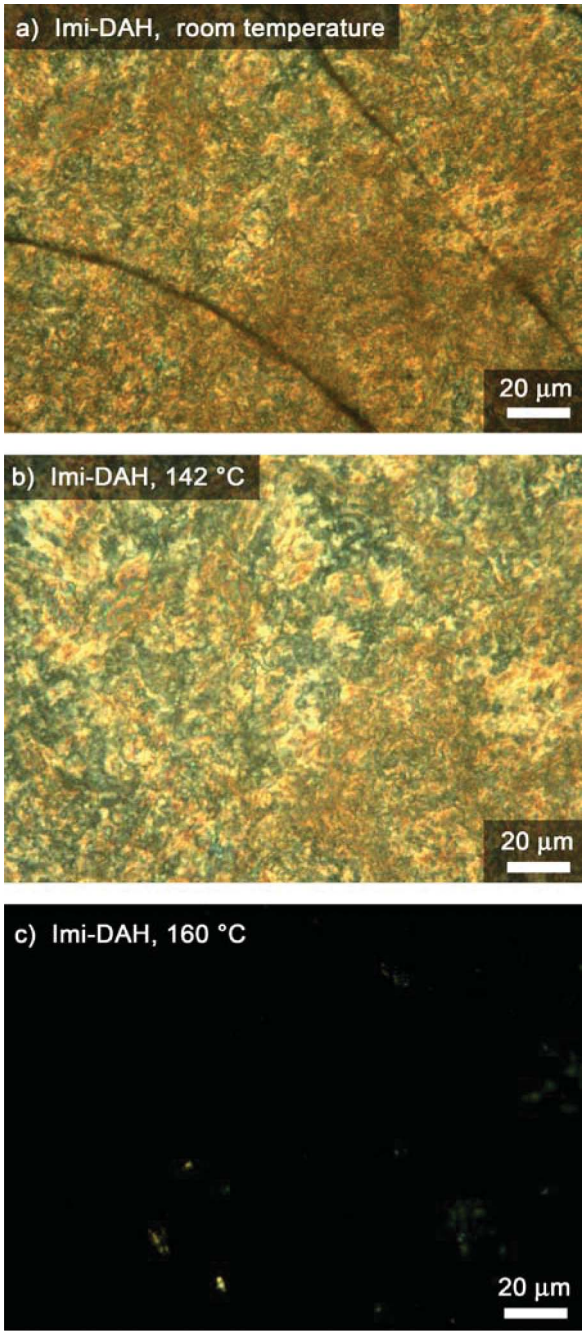

Figure 1. Liquid crystal textures observed by polarising optical microscopy of **Imi-DAH** at: (a) room temperature; (b) 142°C; (c) 160°C.

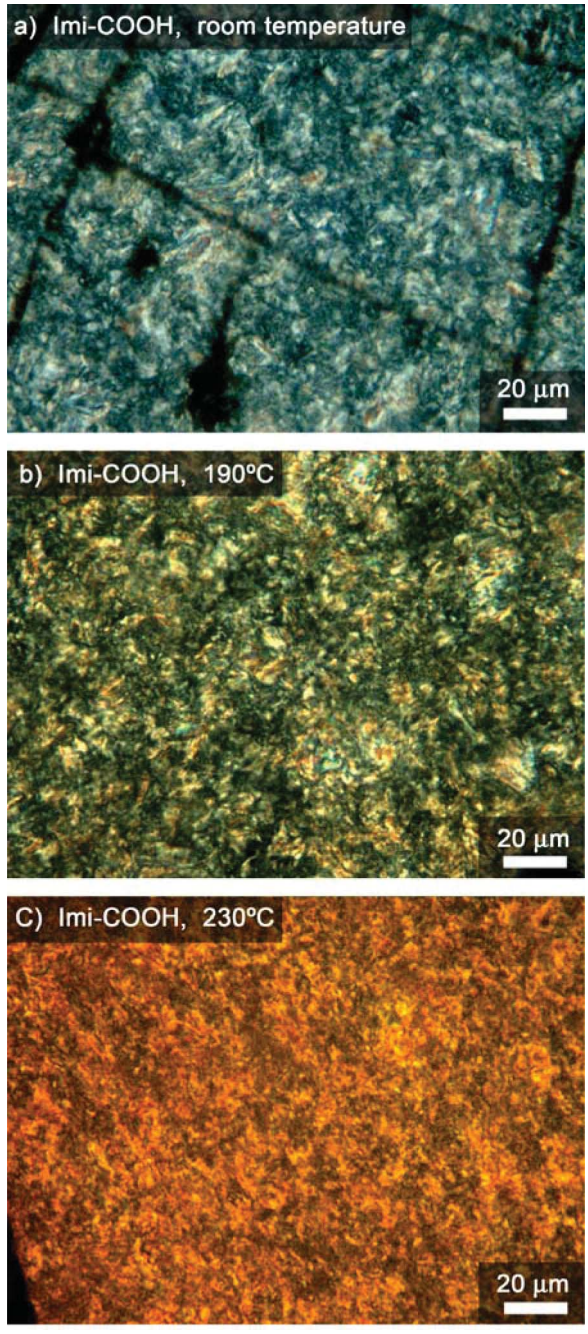

Figure 2. Liquid crystal textures observed by polarising optical microscopy of **Imi-COOH** at: (a) room temperature; (b) 190°C; (c) 230°C.

DSC traces for **Imi-DAH** and **Imi-COOH** are shown in Figure 3. **Imi-DAH** exhibits a melting endotherm around 134°C followed by a clearing endotherm around 151°C. Both transitions were broad and convoluted by weaker endotherms. These features indicate a complicated transition process or, possibly, that the sample is contaminated with small amounts of impurities. Subsequent heating scans indicated that decomposition is not occurring. The DSC trace of **Imi-COOH** shows a sharp endotherm at 170°C that corresponds to melting of the crystalline phase into a mesogenic phase. A much weaker transition presents at 189°C and occurs at the same temperature at which the POM texture changed from the state in Figure 2(b) to that in Figure 2(c). This sample did not show a clearing endotherm below 240°C and, in agreement with LC texture observations, is

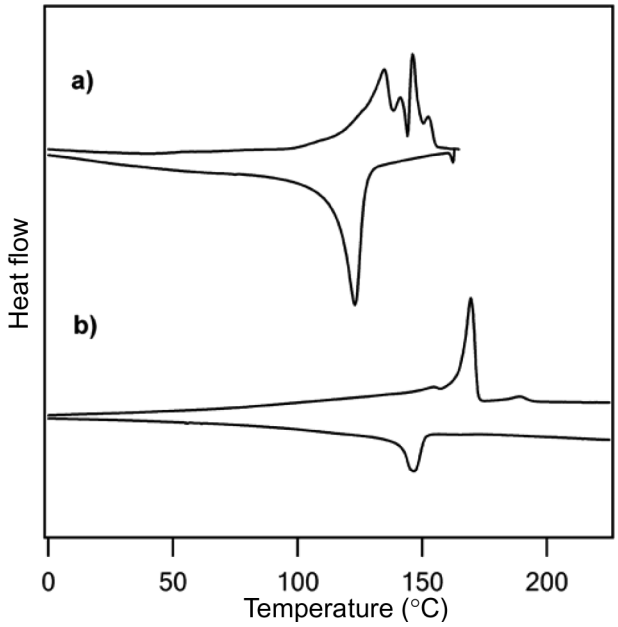

Figure 3. Differential scanning calorimetry scans: (a) **Imi-DAH**; (b) **Imi-COOH**.

suggestive of a high-temperature mesophase. Cooling of **Imi-COOH** only showed a single exotherm corresponding to crystallisation from a super-cooled liquid-crystalline state. Table 1 summarises the DSC transition temperatures and associated enthalpy changes. Phase assignments were made considering XRD data, which will be considered later.

The remarkably high thermal stability of **Imi-COOH**'s mesophase is attributed to hydrogen bond formation between the carboxylic acid ends and to the formation of zwitter-ionic structures, involving hydrogen exchange between the carboxylic acid and the imidazole heterocycle.

In contrast, **Imi-DAH** may also participate in hydrogen bonding, however only through lateral interactions at the diacylhydrazine core. Parra *et al.* [16] synthesised and studied a series of alkyl-terminated diacylhydrazine derivatives and found that longer alkyl chains stabilise smectic C phases. One sample (2g in their manuscript [16]) is identical to **Imi-DAH**, except it does not contain a terminal imidazole group. This sample exhibits a smectic mesophase up to 186°C, significantly higher than the clearing temperature of **Imi-DAH** (150°C). An explanation for the reduced mesophase stability of **Imi-DAH** is that terminal imidazole groups interfere with the lateral hydrogen bonding between diacylhydrazine molecular cores. The imidazole ring offers a secondary amine as a hydrogen bond donor, which can bond with carbonyl groups on the diacylhydrazine core.

Table 1. Transition temperatures and associated enthalpy changes of **Imi-DAH** and **Imi-COOH**.

Compound	Transition	Temperature (°C)	ΔH (J g^{-1})
Imi-DAH	Cr–N	134.1	21.6
	N–I	151.4	6.1
	I–N	171.6	–15.8
	N–Cr	107.6	–36.2
Imi-COOH	Cr–Sm	170.0	75.0
	Sm–Sm'	189.0	2.4
	Sm'–Cr	151.0	–57.9

Note: Cr, crystal; I, isotropic; N, nematic; Sm, smectic.

Figure 4 displays the wide-angle XRD of **Imi-DAH** and **Imi-COOH** obtained following annealing at selected temperatures. For **Imi-DAH**, the data

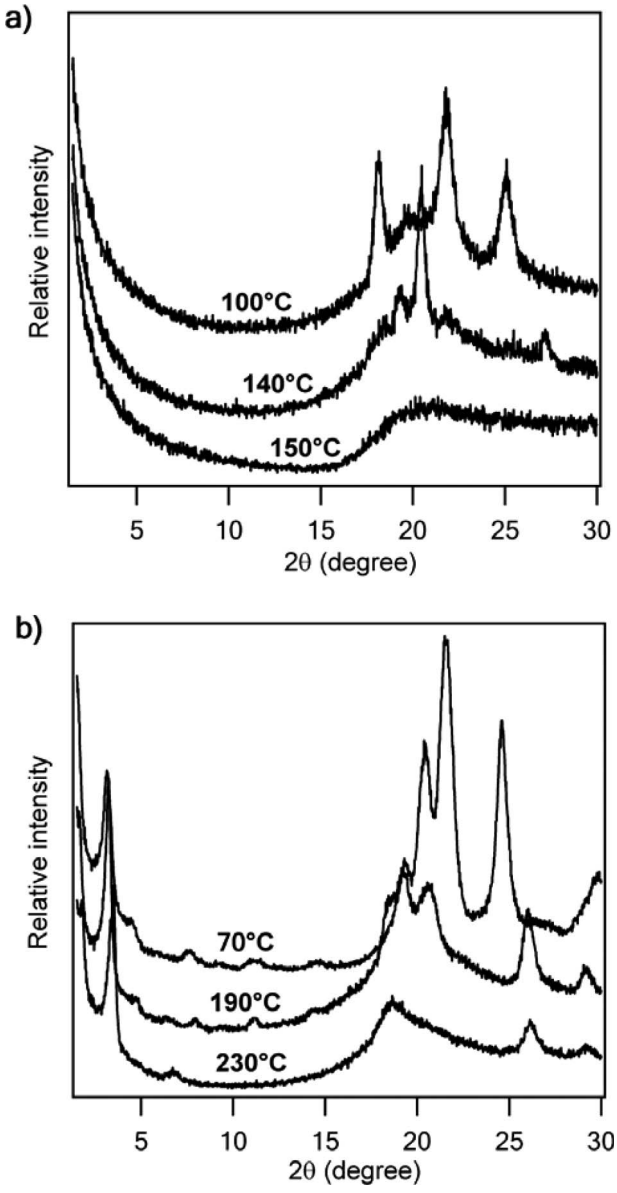

Figure 4. Variable temperature diffractograms: (a) **Imi-DAH**; (b) **Imi-COOH**.

suggest a high-temperature nematic mesophase. The low temperature scan of **Imi-DAH** revealed multiple Bragg peaks, consistent with a highly crystalline structure. Above the sample's melting point, diffuse scattering was observed around $2\theta = 20°$, indicative of the long-range lateral orientational order expected for a typical calamitic mesogen. This scattering results from a periodic length scale of about 4.5 Å. The absence of diffraction peaks at small angles implies that mesogens are not arranged into smectic structures.

In contrast, the diffractograms of **Imi-COOH** support the assignment of a smectic mesophase. At 70°C (beneath the melting point), a crystal structure is evident from the presence of multiple, intense Bragg peaks. Following annealing at 190°C, these peaks shifted in position, were lower in intensity and were significantly broadened, indicating that a phase change to a lower ordered phase had occurred. At this temperature, the presence of a low-angle peak at $2\theta = 3.3°$ is attributed to diffraction of X-rays from smectic layers. This corresponds to an interlayer distance of 27 Å, which agrees with the mesogen's length estimated from a stereomodel of the fully extended conformer (27 Å). More diffuse scattering was observed at larger angles (2θ about 20°) that is due to lateral packing between mesogens within the layers. Subsequent annealing at 230°C led to further reduction of order, however, **Imi-COOH** still showed smectic order consistent with birefringent textures observed using POM.

2.3 *Hydrogen bonding of imidazole end-groups*

Fourier transform infrared (FTIR) spectroscopy was used to study further how terminal imidazole groups affect mesophase behaviour. FTIR spectra at room temperature of **Imi-DAH** and **Imi-COOH** are shown in Figure 5 and peak assignments are presented in Table 2.

Imi-DAH exhibits a broad absorption at 3232 cm^{-1}. This absorption is attributed to N-H stretching vibration and is consistent with the suggestion of Pang and Wang [18] regarding the hydrogen-bonded N-H between diacylhydrazine cores. The presence of this hydrogen-bonded N-H is also supported by the disappearance of free N-H stretching, typically reported as a sharp absorption at frequencies exceeding 3400 cm^{-1}. The expected imidazole N-H absorption (3126 cm^{-1}) is not apparent and may be convoluted into the broad absorption at 3232 cm^{-1}. While carbonyl amide absorption from **Imi-DAH** was observed at 1654 cm^{-1}, it was significantly weaker and broader than expected [18]. A possible explanation for the absence of the imidazole N-H stretch and the broadened carbonyl signal is that the imidazole group interferes with hydrogen bonding between diacylhydrazine groups. The imidazole contains a hydrogen bond acceptor and a hydrogen bond donor, which may bond to both the carbonyl and the amide of the diacylhydrazine group. Hydrogen bonding between acylhydrazines and imidazole groups reduces the lateral ordering between **Imi-DAH** mesogens, leading to the nematic mesophase observed from XRD experiments.

A weak and broad absorption was also observed for **Imi-COOH**'s carbonyl at 1699 cm^{-1} instead of the expected sharp and intense absorption from hydrogen-bonded carboxylic acid dimers [22, 23]. This signal may be broadened due to the presence of multiple hydrogen-bonding scenarios. For example, **Imi-COOH** contains a terminal carboxylic acid

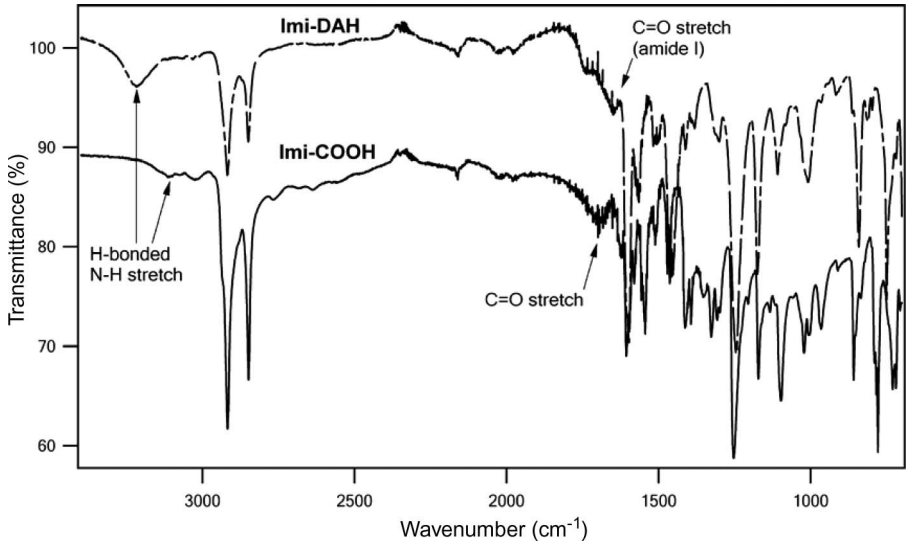

Figure 5. Fourier transform infrared spectra of **Imi-DAH** and **Imi-COOH** at room temperature. Data have been shifted vertically to prevent overlap.

Table 2. Assignments of infrared frequencies of **Imi-DAH** and **Imi-COOH** at room temperature.

	Infrared frequencies (cm^{-1})	
Assignment	**Imi-DAH**	**Imi-COOH**
ν (N–H)	3232, 3126	3131
ν (O–H)	–	3031, 2653
ν (Ar–H)	3049	3044
ν_{as} (CH_3), ν_{as} (CH_2)	2920	2918
ν_s (CH_3), ν_s (CH_2)	2851	2849
amide I, ν(C = O)	1654	–
carboxylic, ν(C = O)	–	1699
ν(C = C) of phenyl ring	1598, 1586	1606, 1590
	1458	1511, 1463
amide II, III, $\nu_{C\text{-}N} + d_{N\text{-}H}$	1518, 1305	–
$(CH_2)_n$ rocking $n \geq 4$	750	731

group and can form head-to-head dimer structures. Alternatively, the presence of a strong basic imidazole ring can promote the formation of a zwitterion structure, consisting of protonated imidazole and deprotonated carboxylate in a head-to-tail fashion [24]. The formation of such zwitterionic structures may explain the unusually high clearing temperatures (>230°C) observed for **Imi-COOH.** This type of intermolecular interaction is similar to that observed between carboxylic acids and nitrogen-containing compounds such as pyridines to form supramolecular LCs [25].

3. Characterisation

^{1}H nuclear magnetic resonance (NMR) spectra were obtained using a Bruker NMR 400 MHz UltraShield FT NMR spectrometer at 400 MHz. Chemical shifts of the signal were quoted relative to $(CH_3)_4Si$ ($\delta = 0.00$) as an internal standard. FTIR measurements were conducted on a 8400s Shimadzu FTIR spectrometer with full internal reflection diamond probe. DSC measurements were performed on a Perkin Elmer DSC 7 connected to a DEC computer via a TAC7/DX thermal analysis controller. The transition temperatures were taken at the maximum of the endothermic and minimum of exothermic peaks. Heating and cooling rates for **Imi-COOH** were 10°C min^{-1} and 5°C min^{-1}, respectively. Heating and cooling rates of **Imi-DAH** were 20°C min^{-1} in both processes. A polarising microscope (Leica DMLP) equipped with a hot stage (Leica Microscope Heating Stage 350) and crossed-polarisers was used for LC texture observations. Variable temperature XRD patterns were investigated with a Philips PW 3710 MPD coupled with Cu K_α diffractometer.

4. Synthesis

Tetradecanedioic acid, N-methylmorpholine, diisopropyl carbodiimide (DIC), N-bromosuccinimide (NBS), and oxalyl chloride were purchased from TCI America (Portland, OR, USA); ethyl chloroformate, hydrobromic acid (47%), benzyl bromide, hydrazine monohydrate from Alfa Aesar; ethyl-4-hydroxy benzoate from Fluka; 2-mercaptoimidazole from Aldrich; sodium borohydride from EMD Chemical (Gibbstown, NJ, USA). All materials were used without further purification.

4.1 Tetradecane diol, 1

Similar to the procedure describe by Nguyen *et al.* [26], to the cold solution of 1 eqv. tetradecanedioic acid in tetrahydrofuran (THF) at −5°C was added 2 eqv. N-methylmorpholine and 2.26 eqv. ethylchloroformate, sequentially and stirred for 15 min. The precipitate of N-methylmorpholine hydrochloride was filtered off. The combined organic solution was introduced into a large flask and 2 eqv. sodium borohydride were added. To assure complete reduction, a slight excess of sodium borohydride was added. After gas evolution had completely ceased, the reaction mixture was poured into water. The solution was filtered, extracted with ethyl acetate, washed with 5% sodium bicarbonate, washed several times with water, and dried over magnesium sulphate to provide the diol product as a white solid. Recrystallisation with hexane and a couple of drops of ethanol provided a pure white crystalline product: melting point (m.p.) 85°C; yield 73%. ^{1}H NMR ($CDCl_3$, 400 MHz): $\delta = 1.20$–1.50 (m, 20 H), 1.63 (quintet (qu), $J = 6$ Hz, 4 H), 3.69 (t, $J = 7$ Hz, 4 H).

4.2 14-Bromotetradecane-1-ol, 2

Following the procedure described in literature [27], a mixture of 1 eqv. diol **1** and 1.2 eqv. of hydrogen bromide (47% in toluene) was refluxed for 72 h, then cooled to room temperature. A solid precipitate was filtered off. The solution was diluted with diethyl ether, washed with 1 M sodium hydroxide, and dried with sodium sulphate. The crude product was purified by column chromatography using an eluent of 1:1 hexane:diethyl ether to separate dibromoalkane and bromoalcohol. The pure bromoalcohol product was recovered as a white soft solid: m.p. 50°C; yield 59%. ^{1}H NMR ($CDCl_3$, 400 MHz): $\delta = 1.20$–1.50 (m, 20 H), 1.63 (qu, $J = 6$ Hz, 2 H), 1.91 (qu, $J = 7$ Hz, 2 H), 3.46 (t, $J = 7$ Hz, 2 H), 3.67 (t, $J = 7$ Hz, 2 H).

4.3 14-(p-Oxy ethyl benzoate)-tetradecane-1-ol, 3

A mixture of 1.2 eqv. ethyl-4-hydroxy benzoate and 3 eqv. potassium carbonate in acetone was refluxed for

30 min. Then, bromoalcohol **2** was added and refluxed further for 24 h. The reaction mixture was cooled, poured into water and acidified with dilute hydrochloric acid until the product precipitated out. The crude product was recrystallised with 1:1 hexane:ethyl acetate to obtain the pure product as a pale yellow soft solid: m.p. 52°C; yield 69%. ^{1}H NMR ($CDCl_3$, 400 MHz): $\delta = 1.30$–1.53 (m, 20 H), 1.43 (t, $J = 7$ Hz, 3 H), 1.60 (qu, $J = 6$ Hz, 2 H), 1.85 (qu, $J = 7$ Hz, 2 H), 3.69 (t, $J = 3$ Hz, 2 H), 4.05 (t, $J = 3$ Hz, 2 H), 4.39 (q, $J = 7$ Hz, 2 H), 6.95 (d, $J = 6$ Hz, 2 H), 8.03 (d, $J = 6$ Hz, 2 H).

4.4 p-(Oxy-14-bromo tetradecyl) ethyl benzoate, 4

A mixture of 1 eqv. substituted benzoate alcohol **3**, 1 eqv. DIC and 1 mol % copper bromide was stirred at room temperature for 2 h. Then, NBS and THF were added to the mixture and refluxed for 8 h [21]. The THF solvent was removed and the crude mixture was washed with water to eliminate copper bromide and DIC. The product was extracted with ethanol and recrystallised in hexane with a small amount of ethanol resulting in pure product as a light brown solid: m.p. 55°C; yield 41%. ^{1}H NMR ($CDCl_3$, 400 MHz): $\delta = 1.30$–1.53 (m, 20 H), 1.43 (t, $J = 7$ Hz, 3 H), 1.85 (qu, $J = 8$ Hz, 2 H), 1.91 (qu, $J = 7$ Hz, 2 H), 3.46 (t, $J = 7$ Hz, 2 H), 4.06 (t, $J = 6$ Hz, 2 H), 4.39 (q, $J = 7$ Hz, 2 H), 6.95 (d, $J = 6$ Hz, 2 H), 8.03 (d, $J = 6$ Hz, 2 H).

4.5 p-(Oxy-14-thiomercapto-2-imidazole tetradecyl) ethyl benzoate, 5

Coupling of mercaptothioimidazole to **4** was similar to the synthesis of **3**, except THF was used as a solvent. The crude was obtained and recrystallised with 1:1 hexane:ethyl acetate. The purified product was obtained as an orange solid: m.p. 58°C; yield 73%. ^{1}H NMR ($CDCl_3$, 400 MHz): $\delta = 1.30$–1.55 (m, 20 H), 1.43 (t, $J = 6$ Hz, 3 H), 1.69 (qu, $J = 8$ Hz, 2 H), 1.85 (qu, $J = 8$ Hz, 2 H), 3.08 (t, $J = 8$ Hz, 2 H), 4.06 (t, $J = 6$ Hz, 2 H), 4.39 (q, $J = 7$ Hz, 2 H), 6.96 (d, $J = 6$ Hz, 2 H), 7.06 (s, 1 H), 7.18 (s, 1 H), 8.03 (d, $J = 6$ Hz, 2 H).

4.6 p-(Oxy-14-thiomercaptoimidazole tetradecyl) benzoic acid, Imi-COOH

A solution of 1 eqv. **5** and 3.75 eqv. potassium hydroxide in 1:4 water:ethanol was refluxed for 4 h. Then, the crude mixture was poured into water and acidified with 1 M hydrochloric acid until the pH was about 4 and a precipitate formed. The precipitate was collected, washed several times with water and dried to obtain **Imi-COOH** as a pale orange solid: m.p. >230°C; yield about 98%. ^{1}H NMR (DMSO-d_6, 400 MHz): $d = 1.30$–1.50 (m, 20 H), 1.56 (qu, $J = 6$ Hz, 2 H), 1.74 (qu, $J = 6$ Hz, 2 H), 3.0 (t, $J = 6$ Hz, 2 H), 4.04 (t, $J = 5$ Hz, 2 H), 6.97 (d, $J = 7$ Hz, 2 H), 7.05 (s, 2 H), 7.88 (d, $J = 7$ Hz, 2 H).

4.7 Benzyloxybenzohydrazide, 7

A mixture of 1 eqv. ethyl-4-hydroxybenzoate and 3 eqv. potassium carbonate in acetone was refluxed for 30 min, 1 eqv. benzyl bromide was added, and the solution was refluxed for a further 3 h. The organic mixture was extracted by chloroform to obtain the crude product **6**. Recrystallisation with 1:1 hexane:ethylacetate resulted in pure product as a white crystalline solid [28]: m.p. 115°C; yield about 80%. One eqv. of **6** was then refluxed with about 8 eqv. of hydrazine monohydrate in ethanol for 10 h. Upon cooling, a precipitate of product **7** formed, producing a light orange crystalline solid: m.p. 140°C; yield 88%. ^{1}H NMR (DMSO-d_6, 400 MHz): $d = 4.38$ (s, 1 H), 5.13 (s, 2 H), 7.03 (d, $J = 8$ Hz, 2 H), 7.31–7.42 (m, 5 H), 7.76 (d, $J = 8$ Hz, 2 H), 9.58 (s, 2 H).

4.8 4-(14-Mercaptylimidazole tetradecyloxy)benzoic acid N′-(4 benzyloxyphenyl-2-carbonyl)hydrazide, Imi-DAH

A solution of **Imi-COOH** 1 eqv. and a couple of drops of dimethylformamide (DMF) in chloroform was cooled to 0°C. Then, 2.7 eqv. of triethylamine and dropwise 3 eqv. of oxalylchloride were added sequentially to the cooled solution. The reaction mixture was warmed to room temperature and stirred further for 3 h. The residual oxalyl chloride was removed under reduced pressure. The obtained crude acid chloride was used in the next step without purification. The next step, crude acid chloride 1 eqv., solution of hydrazide (**7**) 1.2 eqv. and pyridine 1.5 eqv. in DMF was stirred at room temp for 12 h and then poured into a large amount of water. The precipitate was collected and dried in a vacuum oven overnight. The crude product was extracted by ethanol. Purification with column chromatography (5% methanol in chloroform), and precipitated in ethyl acetate produced **Imi-DAH** as a yellow powder: m.p. 150°C; yield 14%. ^{1}H NMR (DMSO-d_6, 400 MHz): $d = 1.30$–1.50 (m, 20 H), 1.56 (qu, $J = 6$ Hz, 2H), 1.75 (qu, $J = 6$ Hz, 2H), 2.98 (t, $J = 6$ Hz, 2 H), 4.07 (t, $J = 5$ Hz, 2 H), 5.23 (s, 2 H), 7.06 (d, $J = 7$ Hz, 2 H), 7.16 (s, 2 H), 7.81 (d, $J = 7$ Hz, 2 H), 10.3 (s, 2 H).

5. Summary

This study highlighted the importance of site-specific hydrogen bonding between molecular parts (e.g. cores

and end-groups) in determining the type and stability of LC mesophase. In summary, two imidazole-terminated mesogens (**Imi-DAH** and **Imi-COOH**) were designed and synthesised. Intermolecular hydrogen bond interactions support the formation of high-temperature (>100°C) LC phases. Hydrogen bonding between **Imi-COOH** promotes a smectic, layered structure, which is sustained at high temperatures (up to 230°C). For **Imi-DAH**, lateral hydrogen-bonding interactions between diacylhydrazine cores were expected to stabilise smectic mesophases, however, a less ordered, nematic mesophase was observed. FTIR analysis of **Imi-DAH** suggests that terminal imidazole groups interfere with hydrogen bonding between diacylhydrazine cores and destabilise the smectic mesophase. Likewise, for **Imi-COOH**, terminal imidazole groups act as both proton donors and acceptors and likely participate in various hydrogen-bonding combinations. This research is a first step in evaluating whether aligned mesophases can be used to engineer anisotropic proton-conductive phases.

Acknowledgements

The authors acknowledge the Royal Thai Government and the University of Rochester's Department of Chemical Engineering for support of this research.

References

[1] Ito-Akita, K.; Nishina, N.; Asai, Y.; Ohno, H.; Ohtake, T.; Takamitsu, Y.; Kato, T. *Polym. Adv. Technol*. **2000**, *11*, 529–533.
[2] Hoshino, K.; Yoshio, M.; Mukai, T.; Kishimoto, K.; Ohno, H.; Kato, T. *J. Polym. Sci., Part A: Polym. Chem*. **2003**, *41*, 3486–3492.
[3] Kosonen, H.; Ruokolainen, J.; Nyholm, P.; Ikkala, O. *Macromolecules (Washington, DC, US)* **2001**, *34*, 3046–3049.
[4] Yoshio, M.; Kato, T.; Mukai, T.; Yoshizawa, M.; Ohno, H. *Mol. Cryst. Liq. Cryst*. **2004**, *413*, 2235–2244.
[5] Mukai, T.; Yoshio, M.; Kato, T.; Yoshizawa-Fujta, M.; Ohno, H. *Electrochemistry (Tokyo, Jpn.)* **2005**, *73*, 623–626.
[6] Kishimoto, K.; Suzawa, T.; Yokota, T.; Mukai, T.; Ohno, H.; Kato, T. *J. Am. Chem. Soc*. **2005**, *127*, 15618–15623.
[7] Saito, Y.; Hirai, K.; Murata, S.; Kishii, Y.; Kii, K.; Yoshio, M.; Kato, T. *J. Phys. Chem. B* **2005**, *109*, 11563–11571.
[8] Shimura, H.; Yoshio, M.; Hoshino, K.; Mukai, T.; Ohno, H.; Kato, T. *J. Am. Chem. Soc*. **2008**, *130*, 1759–1765.
[9] Ruotsalainen, T.; Torkkeli, M.; Serimaa, R.; Makela, T.; Maki-Ontto, R.; Ruokolainen, J.; ten Brinke, G.; Ikkala, O. *Macromolecules (Washington, DC, US)* **2003**, *36*, 9437–9442.
[10] Kreuer, K.D.; Fuchs, A.; Ise, M.; Spaeth, M.; Maier, J. *Electrochim. Acta* **1998**, *43*, 1281–1288.
[11] Schuster, M.; Meyer, W.H.; Wegner, G.; Herz, H.G.; Ise, M.; Schuster, M.; Kreuer, K.D.; Maier, J. *Solid State Ionics* **2001**, *145*, 85–92.
[12] Schuster, M.F.H.; Meyer, W.H.; Schuster, M.; Kreuer, K.D. *Chem. Mater*. **2004**, *16*, 329–337.
[13] Yoon, C.B.; Meyer, W.H.; Wegner, G. *Synth. Met.* **2001**, *119*, 465–466.
[14] Scharfenberger, G.; Meyer, W.H.; Wegner, G.; Schuster, M.; Kreuer, K.D.; Maier, J. *Fuel Cells (Weinheim, Ger.)* **2006**, *6*, 237–250.
[15] Granados-Focil, S.; Woudenberg, R.C.; Yavuzcetin, O.; Tuominen, M.T.; Coughlin, E.B. *Macromolecules (Washington, DC, US)* **2007**, *40*, 8708–8713.
[16] Parra, M.; Hidalgo, P.; Barbera, J.; Carrasco, E.; Saavedra, C. *Liq. Cryst*. **2006**, *33*, 391–397.
[17] Kajitani, T.; Kohmoto, S.; Yamamoto, M.; Kishikawa, K. *Chem. Mater*. **2004**, *16*, 2329–2331.
[18] Pang, D.M.; Wang, H.T.; Li, M. *Tetrahedron* **2005**, *61*, 6108–6114.
[19] Mori, A.; Nimura, R.; Isobe, M.; Takeshita, H. *Chem. Lett*. **1992**, 859–862.
[20] Kreuer, K D. *Chem. Mater*. **1996**, *8*, 610–641.
[21] Li, Z.N.; Crosignani, S.; Linclau, B. *Tetrahedron Lett*. **2003**, *44*, 8143–8147.
[22] Tian, Y.Q.; Xu, X.H.; Zhao, Y.Y.; Tang, X.Y.; Li, T.J.; Sun, J.Z.; Li, C.W.; Pan, A. *Thin Solid Films* **1996**, *285*, 603–605.
[23] Parra, M.; Alderete, J.; Zuniga, C.; Jimenez, V.; Hidalgo, P. *Liq. Cryst*. **2003**, *30*, 297–304.
[24] Lopez, P.; Zaderenko, P.; Balcazar, J.L.; Fonseca, I.; Cano, F.H.; Ballesteros, P. *J. Mol. Struct*. **1996**, *377*, 105–112.
[25] Kato, T.; Mizoshita, N.; Kishimoto, K. *Angew. Chem., Int. Ed*. **2006**, *45*, 38–68.
[26] Nguyen, T.B.; Castanet, A.S.; Nguyen, T.H.; Nguyen, K.P.P.; Bardeau, J.F.; Gibaud, A.; Mortier, J. *Tetrahedron* **2006**, *62*, 647–651.
[27] Chong, J.M.; Heuft, M.A.; Rabbat, P. *J. Org. Chem*. **2000**, *65*, 5837–5838.
[28] Khan, K.M.; Rasheed, M.; Zia-Ullah; Hayat, S.; Kaukab, F.; Choudhary, M.I.; Atta-ur-Rahman; Perveen, S. *Bioorg. Med. Chem*. **2003**, *11*, 1381–1387.